

Where and How to Improve Graph-based Spatio-temporal Predictors

Daniele Zambon^{*1} and Cesare Alippi^{1,2}

¹The Swiss AI Lab IDSIA & Università della Svizzera italiana, Switzerland.

²Politecnico di Milano, Italy.

Abstract

This paper introduces a novel residual correlation analysis, called AZ-analysis, to assess the optimality of spatio-temporal predictive models. The proposed AZ-analysis constitutes a valuable asset for discovering and highlighting those space-time regions where the model can be improved with respect to performance. The AZ-analysis operates under very mild assumptions and is based on a spatio-temporal graph that encodes serial and functional dependencies in the data; asymptotically distribution-free summary statistics identify existing residual correlation in space and time regions, hence localizing time frames and/or communities of sensors, where the predictor can be improved.

1 Introduction

Spatio-temporal predictive models fit the data by leveraging on the inductive bias associated with relational information coming from time and space of the data observations [Bai et al., 2020, Pal et al., 2021, Ruiz et al., 2020, Seo et al., 2018, Wu et al., 2019, Yu et al., 2018]. The spatial domain is typically represented as a graph associated with, *e.g.*, a pixel grid, a 3d mesh, a road map, or a brain network [Li et al., 2018, Shuman et al., 2013, Stankovic et al., 2020]. That said, however, the term *spatial* has to be intended in broader terms referring to any type of functional dependence existing among sensors, well beyond those correlations coming from their physical position. Modern spatio-temporal data, *e.g.*, multivariate time series coming from a sensor network, present us with non-trivial challenges coming from irregular sampling and missing observations, or heterogeneous sensors that can be added or removed from the systems as time progresses Alippi [2014], Montero-Manso and Hyndman [2021]. In this setting, predictive models can display diverse performance in different regions of the space-time, making the analysis of their quality more intricate, yet more relevant to discover unexpected model behaviors and make apparent unattended aspects of the modeled system.

The paper introduces a novel set of methods for analyzing the quality of models trained to solve spatio-temporal prediction tasks. Proposed methods identify if – and, in case, where – designed models failed to learn the data-generating process, and provide guidelines about which parts of the processing pipeline could be improved. Proposed methods rely on the fact that if dependencies are observed in the prediction residuals, *i.e.*, the difference between the target and predicted values, then the given model is not optimal as there is structural information left that the model was not able to capture, leaving margin for improving the prediction performance.

We stress that the analysis of dependencies in the residuals is complementary to that of the prediction error, which observes the loss function scalar value only, and is unable to draw definitive conclusions about model optimality unless the ground-truth model is available or better-performing models have been found, already; differently, what proposed here is very general and does not assume any strong hypothesis that limits the applicability in real-world settings. Otherwise specified, in the

^{*}Corresponding author, daniele.zambon@usi.ch.

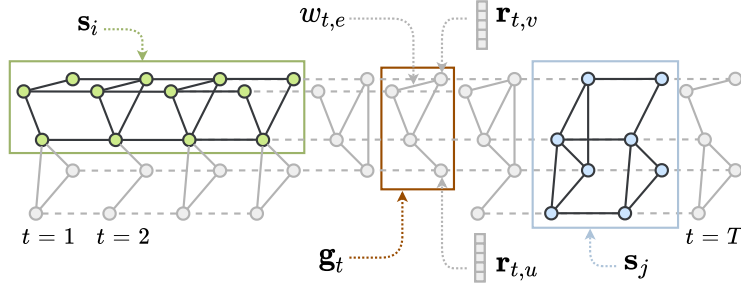


Figure 1: Representation of spatio-temporal data as a sequence of graphs \mathbf{g}_t , $t = 1, 2, \dots, T$; $w_{t,e}$ is the weight of edge e and the prediction residual $\mathbf{r}_{t,v}$ is the signal of node v . Generic subgraphs \mathbf{s}_i and \mathbf{s}_j can be identified for the analysis of residuals.

sequel, “model optimality” is intended in terms of absence of autocorrelation and cross-dependencies among prediction residuals.

The paper aims at answering three main questions:

- Q1** Is the designed model optimal for the prediction problem at hand?
- Q2** Are there space regions (*e.g.*, group of sensors) where predictions can be improved?
- Q3** Are there time periods where the predictor is not optimal?

Above questions can be answered by partitioning the spatial and temporal domains of residuals into subgraphs (as those depicted in Figure 1), and computing appropriate summary statistics, or *scores*, to assess potential correlation existing in there. Scores measure correlation in space and time by leveraging on the AZ-whiteness test setup which neither requires prior knowledge about the data distribution nor identic distributions [Zambon and Alippi, 2022]; accordingly, we name the proposed methods for inspecting the prediction residuals AZ-analysis. The novel paper contribution includes:

- A method to identify nodes whose associated residuals display prominent evidence of correlation [Section 4.2];
- A method to identify time intervals where residuals show evidence of correlation [Section 4.3];
- A method to identify regions of space-time where the correlation of the residuals is more prominent [Section 4.4].
- A comprehensive residual analysis procedure for practitioners [Section 6].

What proposed is extremely versatile. No knowledge about the residuals’ distribution is required, not even that data is identically distributed, only that residuals are centered around zero – an assumption that is readily sidestepped in most scenarios. Moreover, the AZ-analysis can operate on dynamic graphs changing number of nodes and topology over time, with directed or undirected edges, and positive edge weights encoding the strength of the connection.

The paper is structured as follows. Section 2 introduces the edge scores upon which the AZ-analysis is built and shows how to design the spatio-temporal graph, a multiplex graph connecting residual observations according to their spatial and temporal relations. After reviewing the AZ-whiteness test in Section 3, the novel contributions of the paper are presented in Section 4 and validated on synthetic and real data in Sections 5 and 6.

2 Preliminaries

2.1 Spatio-temporal Predictions

Consider a multivariate time series $\mathbf{x} \doteq \{\mathbf{x}_{t,v} : v \in V_t, t = 1, 2, \dots\}$ where $\mathbf{x}_{t,v} \in \mathbb{R}^{d_x}$ is a stochastic vector associated with time step t and sensor v from a sensor set V_t available at time step t ; denote with $V \doteq \bigcup_t V_t$. Consider a family of models f_θ with parameter vector θ trained to predict target $\mathbf{y}_{t,v} \in \mathbb{R}^{d_y}$, for all v, t , from a set of inputs in \mathbf{x} ; exogenous variables, such as information about different types of sensors, are assumed encoded in \mathbf{x} . In a typical time series forecasting task, we have $\mathbf{y}_t = \mathbf{x}_{t:t+H}$, $\hat{\mathbf{y}}_t = f_{\hat{\theta}}(\mathbf{x}_{t-W:t})$ with $\hat{\theta}$ learned to minimize the mean squared error or the mean absolute error between $\hat{\mathbf{y}}_{t,v}$ and $\mathbf{y}_{t,v}$; notation $\mathbf{x}_{a:b}$ indicates $\{\mathbf{x}_t : a \leq t < b\}$. The associate time series of prediction residuals is denoted as $\mathbf{r} = \{\mathbf{r}_{t,v} : \forall v, t\}$ with d_y -dimensional

$$\mathbf{r}_{t,v} \doteq \mathbf{y}_{t,v} - \hat{\mathbf{y}}_{t,v}. \quad (1)$$

In the above time series forecasting example, the i -th component of residual vector $\mathbf{r}_{t,v}$ is associated with the forecast of the i -th next observation $\mathbf{x}_{t+i-1,v}$ at sensor v .

We consider residual data provided along with functional dependencies either known from the application scenario or already extracted directly from the data itself. Relations between sensor pairs at time t are here represented as a graph defined on sensor set V_t as node set and set $E_t \subset V_t \times V_t$ of pairwise relations as edge set. Edges $e \in E_t$ can be directed or undirected and associated with scalar weights $w_{t,e} \in \mathbb{R}_+$; no self-loop is considered, as the focus of the analysis is on discovering dependencies among different spatio-temporal observations. Denote with

$$\mathbf{g}_t = (V_t, E_t, \mathbf{w}_t, \mathbf{r}_t) \quad (2)$$

the attributed graph at time step t with residuals $\mathbf{r}_t \doteq \{\mathbf{r}_{t,v} : v \in V_t\}$ as graph signal and $\mathbf{w}_t \doteq \{w_{t,e} \in \mathbb{R}_+ : e \in E_t\}$ as edge weights. As the node set V_t and the topology E_t can change over time, a graph sequence

$$(\mathbf{g}_1, \mathbf{g}_2, \dots, \mathbf{g}_t, \dots), \quad (3)$$

is generated, *e.g.*, as depicted in Figure 1. Indeed, (3) allows the designer for modeling time series whose relations among sensors are fixed.

2.2 Correlation Assessment through Sign Counts

Following the statistical derivations proposed by Geary [1970] and further developments by Zambon and Alippi [2022], we measure the correlation present in the residuals by counting positive and negative signs

$$\text{sgn}(\mathbf{r}_{t,v}^\top \mathbf{r}_{\tau,u}) \in \{-1, 0, 1\} \quad (4)$$

of the scalar product $\mathbf{r}_{t,v}^\top \mathbf{r}_{\tau,u} = \sum_{i=1}^{d_y} r_{t,v}(i) r_{\tau,u}(i)$ between residual vectors for $(t, v) \neq (\tau, u)$; $\text{sgn}(a)$ equals to $-1, 0$ or 1 depending on whether a is negative, null, or positive.

2.3 Spatio-temporal Graph

A finite sequence $(\mathbf{g}_1, \mathbf{g}_2, \dots, \mathbf{g}_T)$ of length T can be represented as a multiplex graph $\mathbf{g}^* = (V^*, E^*, \mathbf{w}, \mathbf{r})$ by stacking all graphs \mathbf{g}_t , for all $t = 1, 2, \dots, T$, and joining corresponding nodes from consecutive time steps as shown in Figure 1; in the figure, solid gray lines denote edges in \mathbf{g}_t , while dashed gray lines indicate temporal edges added across consecutive graphs. As we see in the sequel, the spatio-temporal graph \mathbf{g}^* provides a convenient static formalization of the observed dynamics.

More specifically, node set V^* of \mathbf{g}^* is defined as

$$V^* \doteq \{v_t \doteq (v, t) : v \in V_t, t = 1, 2, \dots, T\}, \quad (5)$$

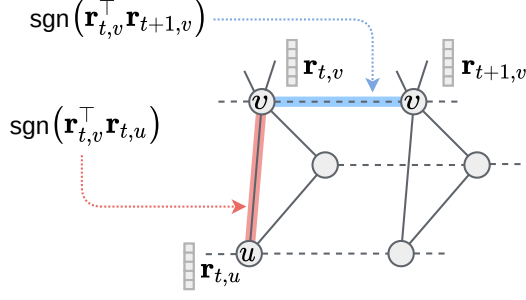


Figure 2: A sector view of the spatio-temporal graph \mathbf{g}^* . Each node is associated with a residual vector. The sign of the inner product between residual vectors of adjacent nodes [Eq. 4] defines the base score of the AZ-analysis. Spatial and temporal edges are treated differently in statistic (11); a spatial edge (v_t, u_t) connecting different nodes at the same time step t is highlighted in red, while a temporal edge (v_t, v_{t+1}) linking corresponding nodes at consecutive time steps in blue.

with each node v_t associated with residual vector $\mathbf{r}_{t,v}$. Graph \mathbf{g}^* is undirected with edge set E^* being the union of two sets

$$E^* \doteq E_{\text{sp}} \cup E_{\text{tm}} \quad (6)$$

where

$$E_{\text{sp}} \doteq \{\{u_t, v_t\} : (u, v) \in E_t, \forall t\}, \quad (7)$$

$$E_{\text{tm}} \doteq \{\{v_t, v_{t+1}\} : v \in V_t \cap V_{t+1}, \forall t\}. \quad (8)$$

Edge set E_{sp} collects all (spatial) edges in sets E_t , for all t , regardless of their direction, if present, while E_{tm} is a set of edges connecting corresponding nodes along the temporal dimension. Note that preserving the direction of edges in \mathbf{g}^* would have no effect in what follows, as we consider statistics derived from (4), which ignores directional information. Finally, if \mathbf{g}_t are undirected, the weight w_{u_t, v_t} of spatial edge $\{u_t, v_t\} \in E_{\text{sp}}$ is set $w_{t, \{u, v\}}$, *i.e.*, the weight corresponding to edge $\{u, v\} \in E_t$. Conversely, for directed graphs \mathbf{g}_t , w_{u_t, v_t} equals $w_{t, (u, v)}$ or $w_{t, (v, u)}$, depending on which one is present in E_t , or $w_{\{u_t, v_t\}} = w_{t, (u, v)} + w_{t, (v, u)}$ if both (u, v) and (v, u) edges are present. The weights for the temporal edges can be defined arbitrarily or, *e.g.*, to balance the overall impact of the spatial and temporal edges, as discussed in Section 3.

3 AZ-whiteness Test

The AZ-analysis presented in this paper relies on the AZ-whiteness test [Zambon and Alippi, 2022], a statistical test defined over the null and alternative hypotheses

$$\begin{cases} H_0 : & \text{All pairs } \mathbf{r}_{t,v}, \mathbf{r}_{\tau,u} \text{ are uncorrelated,} \\ H_1 : & \text{At least a pair } \mathbf{r}_{t,v}, \mathbf{r}_{\tau,u} \text{ is correlated,} \end{cases} \quad (9)$$

for $(t, v) \neq (\tau, u)$, pertaining both autocorrelation and cross-correlation. The test rejects the null hypothesis H_0 any time the absolute value of statistic $C_\lambda(\mathbf{g}^*)$ defined below exceeds a threshold γ set according to a user-defined significance level α

$$\mathbb{P}(|C_\lambda(\mathbf{g}^*)| \geq \gamma \mid H_0) = \alpha. \quad (10)$$

Statistic $C_\lambda(\mathbf{g}^*) \in \mathbb{R}$ is defined as

$$C_\lambda(\mathbf{g}^*) \doteq \frac{\lambda \tilde{C}_{\text{sp}} + (1 - \lambda) \tilde{C}_{\text{tm}}}{(\lambda^2 W_{\text{sp}} + (1 - \lambda)^2 W_{\text{tm}})^{1/2}}; \quad (11)$$

parameter $\lambda \in [0, 1]$ trades off the impact of spatial and temporal components

$$\tilde{C}_{\text{sp}} \doteq \sum_{(u_t, v_t) \in E_{\text{sp}}} w_{\{u_t, v_t\}} \text{sgn}(\mathbf{r}_{t,u}^\top \mathbf{r}_{t,v}), \quad (12)$$

$$\tilde{C}_{\text{tm}} \doteq \sum_{(v_t, v_{t+1}) \in E_{\text{tm}}} w_{\text{tm}} \text{sgn}(\mathbf{r}_{t,v}^\top \mathbf{r}_{t+1,v}), \quad (13)$$

respectively. Scalar w_{tm} is a single weight assigned to all temporal edges and set such that the normalization term $W_{\text{tm}} \doteq |E_{\text{tm}}| \cdot w_{\text{tm}}^2$ equals term W_{sp}

$$W_{\text{sp}} \doteq \sum_{\{u_t, v_t\} \in E_{\text{sp}}} w_{\{u_t, v_t\}}^2. \quad (14)$$

The distinction between spatial and temporal components is also highlighted in Figure 2 with different colors. The intuition behind test statistic (11) is that large positive values of $C_\lambda(\mathbf{g}^*)$ indicate the presence of adjacent residuals similarly oriented, thus suggesting correlation among variables. Similarly, $C_\lambda(\mathbf{g}^*) \ll 0$ provides evidence of negative correlation.

Identifying a value of γ for any choice of α is possible thanks to Theorem 3.1 showing that, asymptotically with the number of edges, $C_\lambda(\mathbf{g}^*)$ follows a standard Gaussian distribution irrespective of the distribution of the residuals and without requesting them to be identically distributed; the theorem is exploited also in the proposed AZ-analysis to ensure summary statistics comparable to each others.

Theorem 3.1. *Consider spatio-temporal graph \mathbf{g}^* with stochastic residuals \mathbf{r} and hyperparameter $\lambda \in [0, 1]$. Assume*

A1 *All residuals $\mathbf{r}_{t,v}$ in \mathbf{r} to be mutually independent and almost surely $\neq \mathbf{0}$,*

A2 *$\mathbb{E}_{\mathbf{r}_{t,v}} [\text{sgn}(\bar{\mathbf{r}}^\top \mathbf{r}_{t,v})] = \mathbf{0}$ for all $\bar{\mathbf{r}} \in \mathbb{R}^{d_y} \setminus \{\mathbf{0}\}$, and $v_t \in V^*$,*

A3 *$w_{\text{tm}}, w_{t,\{u,v\}} \in [w_-, w_+]$ for all $\{u_t, v_t\} \in E_t$ and t , with $0 < w_- < w_+$, then, the distribution of $C_\lambda(\mathbf{g}^*)$ in (11) converges weakly to a standard Gaussian distribution $\mathcal{N}(0, 1)$ as the number $|E^*|$ of edges goes to infinity.*

The proof exploits the central limit theorem under Lindeberg condition and is detailed in the original paper by Zambon and Alippi [2022].

The assumptions of Theorem 3.1 are very mild, thanks also to the choice of assessing correlation by means of the sign (4). More in detail, **A1** is associated with the null hypothesis, while **A2** or **A3** are straightforwardly resolved in most scenarios, if not already fulfilled. In particular, for scalar residuals, **A2** reduces to requesting that the residual median is null. (When **A2** does not hold, residuals should be centered with a suitable offset subtraction.) Offsetting the residuals to meet **A2**, however, is sometimes impossible with $d_y > 1$; in these scenarios, we suggest performing the analysis on each of d_y components independently, eventually aggregating final results. **A3** requests positive bounded weights, as they are assumed to encode the strength of the dependency between the related nodes. In case no weights are given, or they do not fulfill **A3**, we recommend setting all weights to 1.

4 AZ-analysis of Residuals

We design a procedure to set the user’s attention on the most correlated regions of the space-time by analyzing the AZ-whiteness test statistic $C_\lambda(\mathbf{s})$ on appropriately chosen subgraphs \mathbf{s} of spatio-temporal graph \mathbf{g}^* . Given a set $\{\mathbf{s}_i\}_i$ of subgraphs \mathbf{s}_i , Theorem 3.1 ensures that all statistics $C_\lambda(\mathbf{s}_i)$ follow a standard Gaussian distribution – asymptotically¹ and under residuals independence – irrespective of their different node sets, topologies, and edge weights. Thus, statistics $C_\lambda(\mathbf{s}_i)$ can be contrasted to each others, with $|C_\lambda(\mathbf{s}_i)| > |C_\lambda(\mathbf{s}_j)|$ indicating more residual correlation in \mathbf{s}_i than in

¹Note that, as our primary interest is to identify scores deviating from the null distribution. It follows that we do not need large subgraphs to accurately approximate a standard Gaussian; a rough alignment in terms of mean and variance is enough, in the practice.

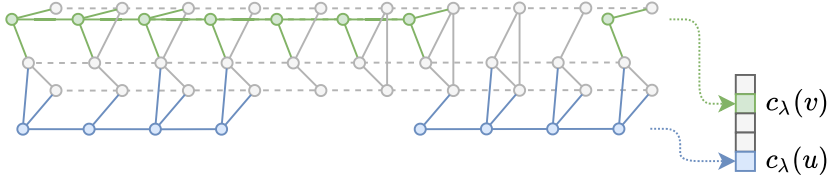


Figure 3: Two generic subgraphs \mathbf{s}_v and \mathbf{s}_u involved in the computation of node-level scores $c_\lambda(v)$ and $c_\lambda(u)$, respectively; the nodes of interest and the related edges are highlighted in color.

\mathbf{s}_j . Accordingly, we suggest to inspect subgraphs associated with scores $|C_\lambda(\mathbf{s}_i)| \gg 0$, starting from the largest ones.

Computing statistics C_λ over all possible subgraphs of \mathbf{g}_* is computationally unfeasible and, moreover, a comprehensive final aggregation of obtained scores would be hard to achieve. In the next sections, we propose principled families of subgraphs leading to straightforward inspection schemes that address **Q1**, **Q2**, and **Q3**.

4.1 Presence of Correlation (Q1)

We assess the overall presence of correlation in the residuals by performing the AZ-whiteness test with $\lambda = 1/2$ and \mathbf{s} being the entire multiplex \mathbf{g}^* . Large values of $|C_{1/2}(\mathbf{g}^*)|$ denote a pronounced correlation in the residuals.

The values of statistics $C_\lambda(\mathbf{g}^*)$ with $\lambda = 0$ and $\lambda = 1$ provide first specific insights about the presence of temporal and spatial correlations, respectively. This follows from Theorem 3.1, as $C_0(\mathbf{g}^*)$ and $C_1(\mathbf{g}^*)$ share the same distribution under the assumption of independent residuals; therefore comparing their values indicates which – temporal or spatial – elements in the processing pipeline show margins for improvement.

For instance, $|C_0(\mathbf{g}^*)| > |C_1(\mathbf{g}^*)|$ with $|C_0(\mathbf{g}^*)| \gg 0$ would imply that autocorrelation is more problematic than the spatial correlation. The designer has to work on the temporal dimension, *e.g.*, by changing the width of the input window or the neural processing layers in the prediction architecture.

4.2 Node-level Analysis (Q2)

To study residuals associated with a subset $\phi \subset V$ of nodes/sensors and tackle request **Q2**, define score

$$c_\lambda(\phi) \doteq C_\lambda(\mathbf{s}_\phi) \quad (15)$$

evaluated on subgraph \mathbf{s}_ϕ of multiplex $\mathbf{g}^* = (V^*, E^*, \mathbf{w}, \mathbf{r})$. Subgraph \mathbf{s}_ϕ is defined by all edges in E^* with at least one ending node related to ϕ , *i.e.*, by all nodes from V^* in set

$$V_\phi^* \doteq \{v_t : v \in \phi \cap V_t, t = 1, \dots, T\} \quad (16)$$

or the associated 1-hop neighborhood

$$N(V_\phi^*) \doteq \bigcup_{v_t \in V_\phi^*} N(v_t); \quad (17)$$

$N(v_t)$ denotes the set of 1-hop neighbors of node v_t . Edges in \mathbf{g}_* linking nodes in $N(V_\phi^*) \setminus V_\phi^*$ are excluded, as they do not directly impact any node of interest $v \in \phi$. Special cases analyzing single nodes v derive from (15) by setting $\phi = \{v\}$, as shown is in Figure 3; with little abuse of notation, denote

$$c_\lambda(v) \doteq c_\lambda(\{v\}). \quad (18)$$

Relevant considerations can be derived from inspecting $c_\lambda(v)$. For example, observing large values of $|c_\lambda(v)|$ when relying on global predictive models, like standard graph neural networks sharing

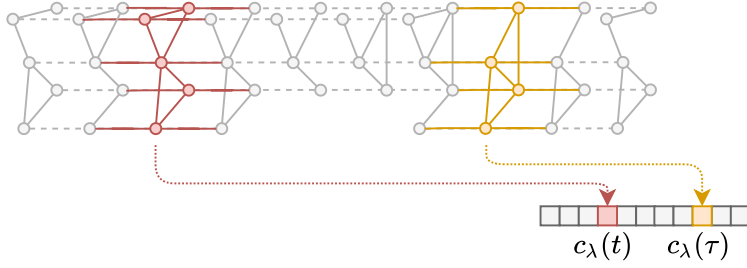


Figure 4: Two generic subgraphs \mathbf{s}_t and \mathbf{s}_τ involved in the computation of temporal scores $c_\lambda(t)$ and $c_\lambda(\tau)$, respectively; the nodes of interest and the related edges are highlighted in color.

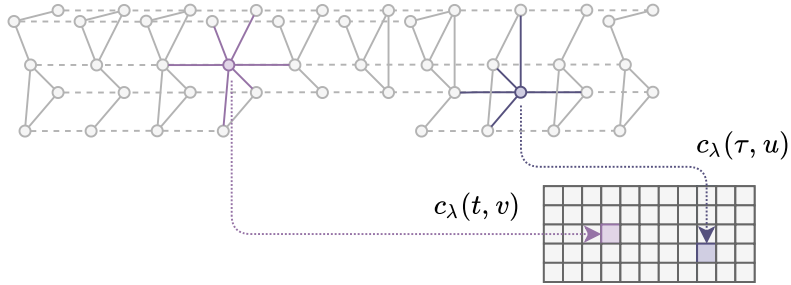


Figure 5: Two generic subgraphs $\mathbf{s}_{t,v}$ and $\mathbf{s}_{\tau,u}$ for $k = 1$ involved in the computation of spatio-temporal scores $c_\lambda(t, v)$ and $c_\lambda(\tau, u)$, respectively; the nodes of interest and the related edges are highlighted in color.

parameters across nodes, can be a warning about the presence of local effects that would be better described by local, node-specific, models.

4.3 Temporal Analysis (Q3)

Assessing request **Q3**, consider subgraphs $\{\mathbf{s}_t\}_t$ slicing multiplex graph \mathbf{g}^* along the temporal axis. For each time step t , we define a score

$$c_\lambda(t) \doteq C_\lambda(\mathbf{s}_t) \quad (19)$$

determined by the subgraph \mathbf{s}_t corresponding to the nodes at time steps $t - 1$, t , and $t + 1$. More specifically, \mathbf{s}_t is the subgraph of \mathbf{g}^* defined by those edges with at least one ending node in

$$V_t^* \doteq \{v_t : v \in V_t\}, \quad (20)$$

as depicted in Figure 4.

Similarly to $c_\lambda(\phi)$ in (15), we can consider a time window $\omega = \{t_1, \dots, t_2\}$, for some $t_1 < t_2$, and construct subgraphs \mathbf{s}_ω from

$$V_\omega^* \doteq \{v_t : v \in V_t, t \in \omega\}, \quad (21)$$

to define statistic

$$c_\lambda(\omega) \doteq C_\lambda(\mathbf{s}_\omega). \quad (22)$$

Discovering time periods associated with large $|c_\lambda(\cdot)|$ might indicate non-stationary behaviors that the model can not properly capture, as shown in Figure 9 below.

4.4 Spatio-temporal Analysis

As the number of nodes and time steps in the data increases, scores (15) and (22) become less effective in discovering correlation existing in localized regions of the space-time; this is a consequence

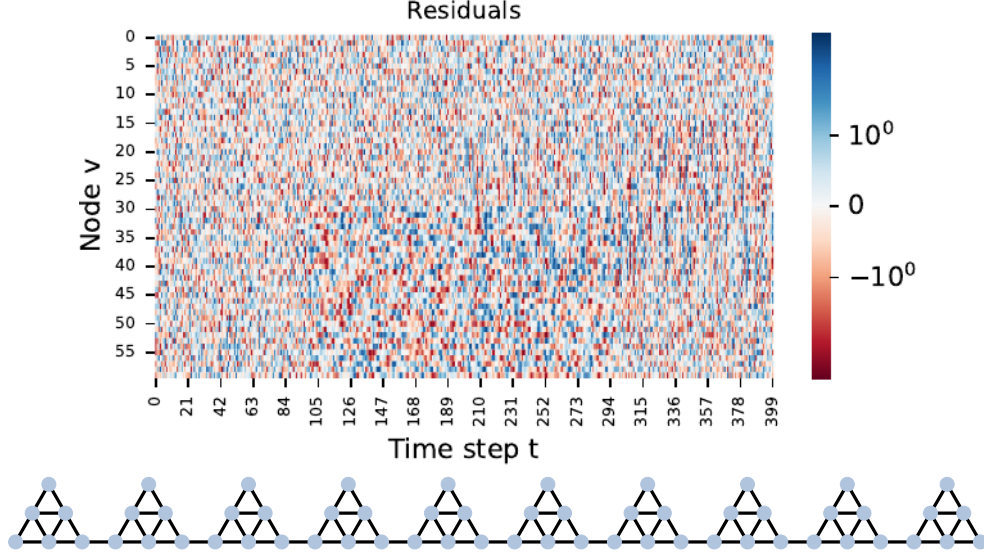


Figure 6: Synthetic residuals and topology of the associated graph; nodes are sorted according to a 1-dimensional spectral embedding.

of $c_\lambda(\phi)$ and $c_\lambda(\omega)$ being averages across all time steps and all nodes, respectively. To address this limit, we present a strategy to identify local correlation patterns across time and space altogether.

For each node $v_t \in V^*$ of \mathbf{g}^* associated with sensor v at time step t , consider statistic

$$c_\lambda(t, v) \doteq C_\lambda(\mathbf{s}_{t,v}), \quad (23)$$

evaluated on $\mathbf{s}_{t,v}$ constructed from the k -hop neighbors of v_t , for some positive k ; see Figure 5. Statistic $c_\lambda(t, v)$ is local in the space-time and accounts for the correlation around (t, v) . For relatively small k , subgraphs $\mathbf{s}_{t,v}$ contain only few edges, making the associated scores $c_\lambda(t, v)$ noisy. Therefore, other than increasing k , we suggest to apply some smoothing filter to $\{c_\lambda(t, v), v \in V, t = 1, \dots, T\}$ interpreted as signal of graph \mathbf{g}^* .

For instance, in the data analyzed in following Sections 5 and 6, we consider $k = 1$ and $L = 5$ iterations of the following spatio-temporal filter

$$z_{t,v}^{l,\text{sp}} = \frac{\sum_{u \in N(v)} z_{t,u}^{l-1} w_{t,\{v,u\}}}{\sum_{u \in N(v)} w_{t,\{v,u\}}} \quad (24)$$

$$z_{t,v}^{l,\text{tm}} = \frac{z_{t-2,v}^{l-1} + z_{t-1,v}^{l-1}}{2} \quad (25)$$

$$z_{t,v}^l = \frac{z_{t,v}^{l-1} + \lambda z_{t,v}^{l,\text{sp}} + (1 - \lambda) z_{t,v}^{l,\text{tm}}}{2} \quad (26)$$

for $l = 1, \dots, L$, starting from $z_{t,v}^0 = c_\lambda(t, v)$; we denote the resulting scores as

$$\bar{c}_\lambda(t, v) \doteq z_{t,v}^L. \quad (27)$$

5 Empirical Validation of the Score Behavior

The first experiment considers a synthetic dataset where we artificially introduced temporal and spatial correlation to show that the proposed scores $c_\lambda(\cdot)$ are indeed able to detect correlation patterns.

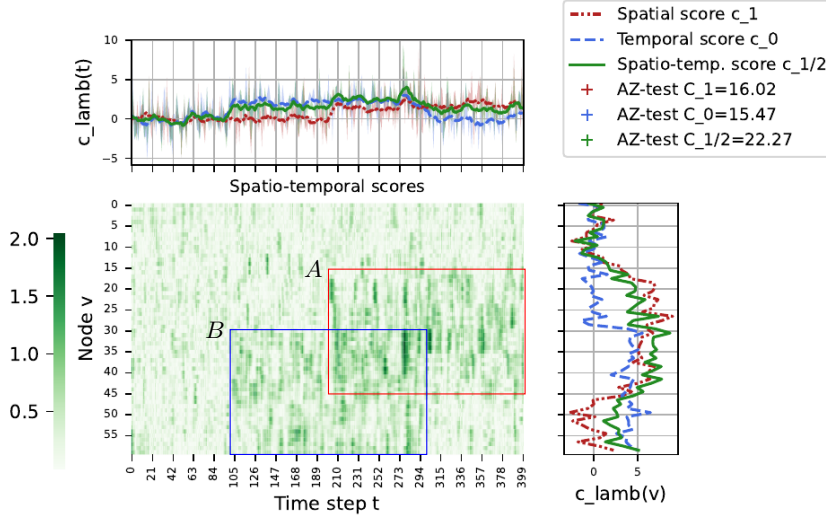


Figure 7: Visualization of the statistics $C_\lambda(\mathbf{g}^*)$ (in the legend) and scores $c_\lambda(v)$, $c_\lambda(t)$ and $c_\lambda(t, v)$ involved in the AZ-analysis of residuals on synthetic data. Bottom left) Absolute value $|\bar{c}_{1/2}(t, v)|$. Top left) Temporal scores $c_\lambda(t)$; a moving average is applied to improve readability. Bottom right) Node-level scores $c_\lambda(v)$. The red (blue) box represents set A (B) associated with spatial (temporal) correlation.

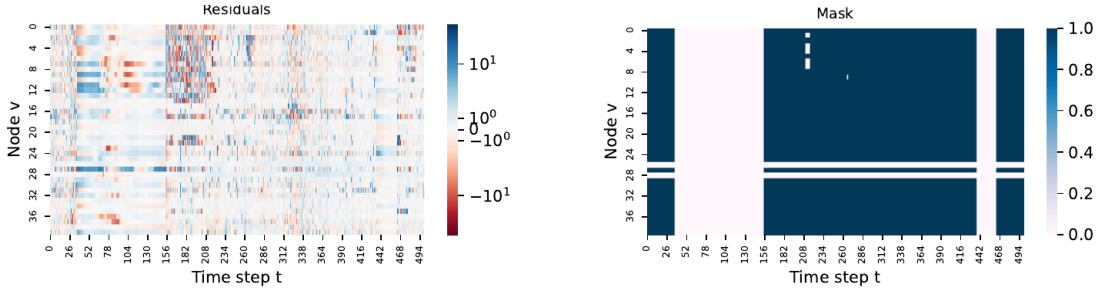


Figure 8: Residuals obtained on MetrLA dataset with imputed data and associated mask with 0 and 1 meaning missing and available data, respectively.

Synthetic residuals The considered residual signal \mathbf{r} is generated from an i.i.d. white noise $\varepsilon_{t,v} \sim \mathcal{N}(0, 1)$, $t = 0, \dots, 399$ and $v = 0, \dots, 59$, associated with the graph of Figure 6. Nodes and time steps are divided into four regions determined by sets $A \doteq \{200, \dots, 399\} \times \{15, \dots, 44\}$ presenting spatial correlation and $B \doteq \{100, \dots, 299\} \times \{30, \dots, 59\}$ associated with temporal correlation. For each (t, v) outside $A \cup B$, the synthetic residual $r_{t,v} \in \mathbb{R}$ is uncorrelated and set to $\varepsilon_{t,v}$. $A \setminus B$ is a region of only spatial correlation, with

$$r_{t,v} = \varepsilon_{t,v} + \frac{\sum_{u \in N(v)} \varepsilon_{t,u}}{|N(v)|}, \quad (28)$$

while in $B \setminus A$ only temporal correlation is present

$$r_{t,v} = \varepsilon_{t,v} + \frac{\varepsilon_{t-1,u} + \varepsilon_{t+1,u}}{2}. \quad (29)$$

Finally, both spatial and temporal correlations are introduced:

$$r_{t,v} = \varepsilon_{t,v} + \frac{\sum_{u \in N(v)} \varepsilon_{t,u}}{|N(v)|} + \frac{\varepsilon_{t-1,u} + \varepsilon_{t+1,u}}{2}, \quad (30)$$

in $A \cap B$.

Analysis of residuals In Figure 7, we observe that the values of the AZ-whiteness test statistics $C_\lambda(\mathbf{g}^*)$ are substantially larger than 0, correctly identifying the presence of both spatial and temporal correlation. Secondly, the magnitude of all node-level scores $c_1(v)$ and temporal scores $c_1(t)$ (red dot-dashed lines) are consistent with set A containing spatial correlation. Similarly, $c_0(v)$ and $c_0(t)$ (blue dashed lines) are consistent with B associated with temporal correlation. $c_{1/2}(v)$ and $c_{1/2}(t)$ (green solid lines) are consistent with the union set $A \cup B$. Moreover, scores $c_{1/2}(\cdot)$ are larger where both types of correlation are present ($A \cap B$), than where there is only either of the two ($A \setminus B$ and $B \setminus A$). Lastly, $|\bar{c}_{1/2}(t, v)|$ are overall larger within region $A \cup B$.

6 Use Case in Traffic Forecasting

In the second experiment, we analyze the prediction residuals of a spatio-temporal graph neural network (STGNN) trained to solve 1-step ahead forecasting on traffic data.

Data and model The considered data is the MetrLA traffic dataset Li et al. [2018] which aggregated traffic information into 5-minute intervals of sensor readings between March 2012 and June 2012. A graph connecting the sensors is constructed from their pairwise distance. The considered predictive model is a time-then-space STGNN Gao and Ribeiro [2022] based on Satorras et al. [2022] and detailed in the appendix. The model is trained to minimize the mean absolute error (MAE) on 1h-ahead predictions on the first 70% of data appropriately masking the missing observations (about 8% of the data), validated on the following 10%, and tested on the remaining 20%; as a reference with the literature – *e.g.*, see Wu et al. [2019] – the obtained test MAE at 15min, 30min, and 1h are 2.74, 3.14, and 3.61, respectively.

In Figure 9, we perform the proposed AZ-analysis on prediction residuals obtained following two setups. The first one considers the test set appropriately masked, the second one considers the time series with the missing data imputed by replicating the last available observation. In the remainder of the section, we comment on the relevant insights derived from the analysis; for space constraints, only 1-step ahead prediction residuals within the 40-node 500-time steps window shown in Figure 8 is analyzed.

Presence of correlation The AZ-whiteness test run with different λ values on the properly masked test data (panel on the left, Figure 9) evidenced correlated residuals ($C_{1/2}(\mathbf{g}^*) = 54.53$), and shows that the spatial correlation ($C_1(\mathbf{g}^*) = 72.15$) is more prominent than the temporal one ($C_0(\mathbf{g}^*) = 4.96$); in agreement with above comment, we observe that scores $c_1(t)$ and $c_1(v)$, *i.e.*, those accounting only for the spatial edges, are substantially different from 0 for most of the time steps t and nodes v , whereas $c_0(t)$ and $c_0(v)$ fluctuate around 0.

Node-level and temporal analyses Analyzing the residuals on the test set with imputed data (panel on the right, Figure 9), we observe two distinct time intervals where the temporal scores $c_\lambda(t)$, for $\lambda = 0$ and $\frac{1}{2}$, are large; similarly, it is evident that $c_0(v)$ for $v = 26$ and 28 takes larger values than other nodes. As we can see from the mask of the missing/imputed data shown in Figure 8, the identified nodes and time steps are all associated with artificially imputed data and, most likely, the observed large scores are linked to the considered imputation method of replicating the last observed value. Conversely, scores $c_1(\cdot)$ are compatible with those observed in the left panel of Figure 9. We conclude that the proposed scores are able to detect changes in the data-generating process, and trigger warnings about the model validity in the new operating conditions.

Spatio-temporal analysis By the analysis of $\bar{c}_{1/2}(t, v)$ in Figures 9, *i.e.*, scores $c_{1/2}(t, v)$ filtered according to (24)-(26), problematic space-time regions are apparent and consistent with the analysis carried out up to here (*e.g.*, see the scores in time interval $40 \leq t < 156$), and display other localized regions of correlated residuals, like that around time step $t = 230$.

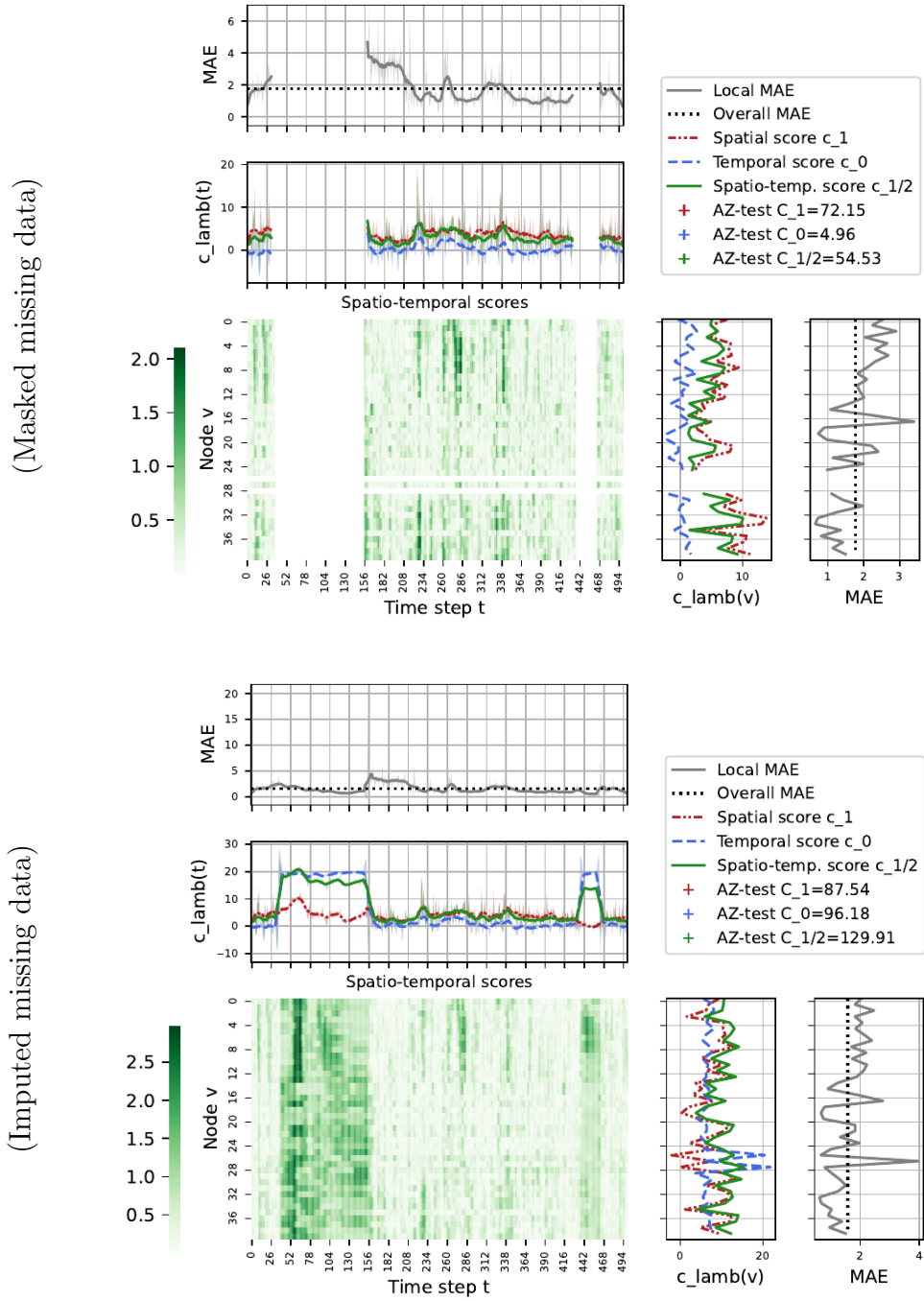


Figure 9: Visualization of the statistics $C_\lambda(\mathbf{g}^*)$ and scores $c_\lambda(v)$, $c_\lambda(t)$ and $c_\lambda(t, v)$ involved in the AZ-analysis on MetrLA dataset. The top and bottom panels report the analysis with missing data appropriately masked and with imputed missing data, respectively. In each panel: Bottom left) Absolute value $|\bar{c}_{1/2}(t, v)|$ computed from $c_{1/2}(t, v)$; set to 0 in masked regions. Top left) MAE and scores $c_\lambda(t)$ associated with time step t ; a moving average is applied to improve readability. Bottom right) MAE and scores $c_\lambda(v)$ associated with node v . The legend reports the AZ-whiteness test statistics $C_\lambda(\mathbf{g}^*)$. Nodes are sorted according to a 1-dimensional spectral embedding.

Absolute error and residual correlation Finally, we comment that the phenomena highlighted above are not noticeable from the analysis of the MAE provided in Figure 9, indicating that correlation may be present even if the prediction error appears small or coherent with rest of the data.

We conclude that the presented analysis of residuals is complementary to an analysis of the prediction error and provides extremely valuable insights about the tackled machine-learning problem and solution.

7 Conclusions

In this paper, we introduce a novel analysis of model prediction residuals, called AZ-analysis, for spatio-temporal data that allows practitioners to identify space-time regions, such as time intervals or sets of sensors, where the model performance can be improved. The proposed analysis complements that of the prediction error by evaluating the presence of temporal and spatial residual correlation in regions of the space-time and sheds light on aspects where the predictive model is not optimal. The AZ-analysis is well-suited for real-world scenarios as it scales to large and complex datasets by exploiting graph-side information, and only requests residuals centered around zero in a few setups; no other assumption about the distribution of residuals is requested, not even of identic distribution. General comments on how to interpret the results are provided along with a real-world use case in the context of traffic forecasting to showcase the potential of the proposed AZ-analysis.

Acknowledgements

This work was supported by the Swiss National Science Foundation project FNS 204061: *High-Order Relations and Dynamics in Graph Neural Networks*.

References

- C. Alippi. *Intelligence for embedded systems*. Springer, 2014.
- L. Bai, L. Yao, C. Li, X. Wang, and C. Wang. Adaptive graph convolutional recurrent network for traffic forecasting. *Advances in neural information processing systems*, 33:17804–17815, 2020.
- A. Cini and I. Marisca. Torch Spatiotemporal, 3 2022. URL <https://github.com/TorchSpatiotemporal/tsl>.
- M. Fey and J. E. Lenssen. Fast Graph Representation Learning with PyTorch Geometric, 5 2019. URL https://github.com/pyg-team/pytorch_geometric.
- J. Gao and B. Ribeiro. On the equivalence between temporal and static equivariant graph representations. In *International Conference on Machine Learning*, pages 7052–7076. PMLR, 2022.
- R. C. Geary. Relative efficiency of count of sign changes for assessing residual autoregression in least squares regression. *Biometrika*, 57(1):123–127, 04 1970. ISSN 0006-3444. doi: 10.1093/biomet/57.1.123.
- C. R. Harris, K. J. Millman, S. J. van der Walt, R. Gommers, P. Virtanen, D. Cournapeau, E. Wieser, J. Taylor, S. Berg, N. J. Smith, R. Kern, M. Picus, S. Hoyer, M. H. van Kerkwijk, M. Brett, A. Haldane, J. F. del Río, M. Wiebe, P. Peterson, P. Gérard-Marchant, K. Sheppard, T. Reddy, W. Weckesser, H. Abbasi, C. Gohlke, and T. E. Oliphant. Array programming with NumPy. *Nature*, 585(7825):357–362, Sept. 2020. doi: 10.1038/s41586-020-2649-2. URL <https://doi.org/10.1038/s41586-020-2649-2>.
- Y. Li, R. Yu, C. Shahabi, and Y. Liu. Diffusion convolutional recurrent neural network: Data-driven traffic forecasting. In *International Conference on Learning Representations*, 2018. URL <https://openreview.net/forum?id=SJiHXGWAZ>.

- P. Montero-Manso and R. J. Hyndman. Principles and algorithms for forecasting groups of time series: Locality and globality. *International Journal of Forecasting*, 37(4):1632–1653, 2021.
- S. Pal, L. Ma, Y. Zhang, and M. Coates. Rnn with particle flow for probabilistic spatio-temporal forecasting. In *International Conference on Machine Learning*, pages 8336–8348. PMLR, 2021.
- L. Ruiz, F. Gama, and A. Ribeiro. Gated graph recurrent neural networks. *IEEE Transactions on Signal Processing*, 68:6303–6318, 2020.
- V. G. Satorras, S. S. Rangapuram, and T. Januschowski. Multivariate time series forecasting with latent graph inference. *arXiv preprint arXiv:2203.03423*, 2022.
- Y. Seo, M. Defferrard, P. Vandergheynst, and X. Bresson. Structured sequence modeling with graph convolutional recurrent networks. In *International conference on neural information processing*, pages 362–373. Springer, 2018.
- D. I. Shuman, S. K. Narang, P. Frossard, A. Ortega, and P. Vandergheynst. The emerging field of signal processing on graphs: Extending high-dimensional data analysis to networks and other irregular domains. *IEEE signal processing magazine*, 30(3):83–98, 2013.
- L. Stankovic, D. Mandic, M. Dakovic, M. Brajovic, B. Scalzo, S. Li, and A. G. Constantinides. Graph signal processing—part iii: Machine learning on graphs, from graph topology to applications. *arXiv preprint arXiv:2001.00426*, 2020.
- Z. Wu, S. Pan, G. Long, J. Jiang, and C. Zhang. Graph wavenet for deep spatial-temporal graph modeling. In *The 28th International Joint Conference on Artificial Intelligence (IJCAI)*. International Joint Conferences on Artificial Intelligence Organization, 2019.
- B. Yu, H. Yin, and Z. Zhu. Spatio-temporal graph convolutional networks: a deep learning framework for traffic forecasting. In *Proceedings of the 27th International Joint Conference on Artificial Intelligence*, pages 3634–3640, 2018.
- D. Zamboni and C. Alippi. AZ-whiteness test: a test for signal uncorrelation on spatio-temporal graphs. In A. H. Oh, A. Agarwal, D. Belgrave, and K. Cho, editors, *Advances in Neural Information Processing Systems*, 2022. URL <https://openreview.net/forum?id=SFekNSxect>.

A Hardware and Software

Model training and inference are performed on a workstation equipped with Intel(R) Xeon(R) Silver 4116 CPU 2.10GHz processors and NVIDIA TITAN V GPUs. The analysis of residuals does not require GPU acceleration. Experiments are developed in Python 3.8 mainly relying on open-source libraries Pytorch Geometric Fey and Lenssen [2019], Torch Spatiotemporal Cini and Marisca [2022] and NumPy Harris et al. [2020].

The source code to reproduce the results will be released upon publication.

B Spatio-temporal Predictor

The predictive model considered in the traffic forecasting experiment of Section 6 is a spatio-temporal graph neural network composed of encoder, message-passing, and readout modules. The encoder is implemented as a 3-layer multilayer perceptron (MLP) with sigmoid linear unit (SiLU) as activation between layers

$$\mathbf{z}_{t,v} = \text{ENC}(\mathbf{x}_{t-W:t,v}) \quad (31)$$

applied to each node $v \in V$. The message-passing module is 2-layer

$$\mathbf{h}_t = \text{MP}(\{\mathbf{z}_{t,v} \parallel \mathbf{e}_v\}_v, \mathbf{A}), \quad (32)$$

with $\mathbf{e}_v \in \mathbb{R}^{64}$ trainable node embeddings. Finally, the node-wise readout

$$\hat{\mathbf{y}}_{t,v} = \text{READOUT}(\mathbf{h}_{t,v}) \quad (33)$$

is a 2-layer MLP with SiLU activation and linear output. In particular, the message-passing layers have gated messages

$$\begin{aligned} \hat{\mathbf{m}}_{u,v}^{l-1} &= \text{MSG}(\mathbf{h}_{t,v}^{l-1} \parallel \mathbf{h}_{t,u}^{l-1}) \\ \mathbf{m}_{u,v}^{l-1} &= \text{GATE}(\hat{\mathbf{m}}_{u,v}^{l-1}) \cdot \hat{\mathbf{m}}_{u,v}^{l-1} \end{aligned}$$

with MSG a 2-layer MLP with SiLU activations and GATE a scalar linear layer with sigmoid activation; $\mathbf{h}_{t,v}^0$ being the input from (32). The node representations are updated with a 2-layer MLP with SiLU activation, linear output and a skip connection

$$\mathbf{h}_{t,v}^l = \text{UPDATE}\left(\mathbf{h}_{t,v}^{l-1} \parallel \sum_{u \in N(v)} \mathbf{m}_{u,v}^{l-1}\right) + \mathbf{h}_{t,v}^{l-1}.$$

The hidden units per layer are 64. The inputs include exogenous variables encoding the time of the day. The model is trained to minimize the MAE for 12-step ahead predictions (1 hour) from a window of 12-time steps in the past. The training is performed for 200 epochs with Adam optimizer, a cosine annealing scheduler from learning rate 0.005 and 0.0001, and a batch size of 16; early stopping is triggered on the validation MAE with patience of 50 epochs.